arXiv:1510.04793v1 [physics.class-ph] 16 Oct 2015

Analytical determination of the attack transient in a clarinet with time-varying blowing pressure

A. Almeida[a,b,*], B. Bergeot[a,c], C. Vergez[c] and B. Gazengel[a]

[a] *LUNAM Université, Université du Maine, UMR CNRS 6613, Laboratoire d'Acoustique, Avenue Olivier Messiaen, 72085 Le Mans Cedex 9, France*

[b] *School of Physics, The University of New South Wales, Sydney UNSW 2052, Australia*

[c] *LMA, CNRS UPR7051, Aix-Marseille Univ., Centrale Marseille, F-13402 Marseille Cedex 20, France*

Abstract

This article uses a basic model of a reed instrument, known as the lossless Raman model, to determine analytically the envelope of the sound produced by the clarinet when the mouth pressure is increased gradually to start a note from silence. Using results from dynamic bifurcation theory, a prediction of the amplitude of the sound as a function of time is given based on a few parameters quantifying the time evolution of mouth pressure. As in previous uses of this model, the predictions are expected to be qualitatively consistent with simulations using the Raman model, and observations of real instruments. Model simulations for slowly variable parameters require very high precisions of computation. Similarly, any real system, even if close to the model would be affected by noise. In order to describe the influence of noise, a modified model is developed that includes a stochastic variation of the parameters. Both ideal and stochastic models are shown to attain a minimal amplitude at the static oscillation threshold. Beyond this point, the amplitude of the oscillations increases exponentially, although some time is required before the oscillations can be observed at the "dynamic oscillation threshold". The effect of a sudden interruption of the growth of the mouth pressure is also studied, showing that it usually triggers a faster growth of the oscillations.

*Corresponding author: andre.almeida@univ-lemans.fr

1 Introduction

One of the many skills involved in learning how to play the clarinet is to control the attack of a new note. Tonguing is an important aspect of a clear and precise attack, but the evolution of the mouth pressure during the first instants of the note is also seen to affect the attack considerably. Moreover, in some particular situations, tonguing may not be involved in starting a new note. Hence there is both scientific and practical interest in the question: what combinations of tonguing and evolution of the blowing pressure produces sharp and precise attacks?

As a self-sustained musical instrument, the clarinet can be seen as a dynamic system in which the oscillation is controlled by input parameters from the musician. Two of the most important [1, 2, 3] are the blowing pressure and the lip force upon the reed. Models predict the range of parameter values that allow for the production of a musical note [4]. Other useful predictions are the dependence of amplitude of oscillation on these two parameters, period doubling bifurcation points [5, 6], or the parameter regions where the reed touches the lay of the mouthpiece. [7, 8].

More complex models exist that can simulate the reed oscillation in time-domain [9] or harmonic balance methods [10]. They provide more accurate predictions but their complexity makes it hard to grasp the causality relation between parameters and conse-

quences in oscillatory behaviour.

In previous studies in which mouth pressure was gradually increased at constant rates, oscillations appeared at a much higher mouth pressure threshold than that predicted assuming a constant mouth pressure. High thresholds were observed in an artificially blown clarinet [11] and even higher in numerical simulations [12].

Analytical reasoning [13] based on dynamic bifurcation theory [14, 15] predicts a delay in the threshold of oscillation for a linearly increasing mouth pressure, but the exact value of mouth pressure at which it occurs is only valid for simulations performed with very high precision. The threshold observed with normal precision simulations can only be explained with a modified theory [16] using stochastic perturbations [14].

This article extends previous studies by the present authors by switching the focus from the threshold of oscillation to a complete description of the amplitude of oscillation. A simplified model of a note attack is a constant increase in the mouth pressure (as used in previous articles) which ceases increasing and then remains constant at a defined value. The effect of ceasing the pressure increase is studied analytically to develop a full recipe for estimating the envelope of the attack. This recipe is then explored by comparing to actual simulations of the Raman model.

In section 2, the model of the clarinet used in this work is briefly presented, as well as some of its known properties. The remaining of this section provides a brief overview of the key concepts that are needed for the present article (most of these concepts are described with more details in two articles by the authors [13, 16]). Section 3 describes the calculation of the envelope of the oscillations relative to the invariant curve, firstly in an ideal case with infinite precision, then with limited precision or noise (section 3.3). To some extent, these methods were already employed in previous articles [13, 16] to determine a dynamic threshold of oscillation. Here they are extended to calculate the envelope before this threshold is reached. Section 4 presents a method to take into account a discontinuity in the time derivative of the mouth pressure. In section 5, the models are applied to particular examples and simulations, analysing the consequences in terms of expected evolution of the sound. A list of the symbols used in this article is provided in Appendix A.

2 Elements of clarinet theory

2.1 The clarinet model

For an elementary analysis, the clarinet can be described using a version of the lossless Raman model [17], originally used for the bowed string. The system is described by two state variables p and u, made non-dimensional by dividing them respectively by the minimum pressure that closes the reed in steady-state, and the maximum flow allowed by the reed valve. A non-linear function $u = F(p)$ relates the pressure difference between the mouth and the mouthpiece ($\Delta p = \gamma - p$, where γ is the mouth pressure) to the volume of air that flows past the reed (u). The derivation of this formula is given for instance by Chaigne and Kergomard [18].

$$F(p) = \begin{cases} \zeta\,(\Delta p - 1)\,\sqrt{-\Delta p} & \text{if } \Delta p < 0; \quad \text{(1a)} \\ \zeta\,(1 - \Delta p)\,\sqrt{\Delta p} & \text{if } \Delta p \in [0, 1]; \quad \text{(1b)} \\ 0 & \text{if } \Delta p > 1. \quad \text{(1c)} \end{cases}$$

The control parameters of the system are the mouth pressure γ and the embouchre parameter $\zeta = \frac{\rho c}{S_{res}} S \sqrt{\frac{2P_M}{\rho}} \frac{1}{P_M}$. ζ is related the lip force via the opening area of the reed at rest S and is proportional to the characteristic impedance at the resonator input $\frac{\rho c}{S_{res}}$. Three examples of the function F (Fig. 1(a)) show that smaller values of ζ bring the characteristic function closer to that of a stopped pipe ($u = 0$). Increasing γ shifts the curve along the p-axis.

The reed-mouthpiece system drives the resonator. It is linked to it by the acoustic variables p and u found in Eq. (1). For a time-domain description it is usually simpler to describe the resonator using two non-dimensional traveling wave variables x and y, respectively the outgoing and incoming pressure

waves:

$$p(t) = x(t) + y(t),$$
$$u(t) = x(t) - y(t). \quad (2)$$

The incoming wave $y(t)$ at the bore input is the opposite of the delayed outgoing wave $-x(t-\tau)$, since no losses in the propagation or reflection are considered[1]. In practice, only one value of $x(t)$ is calculated in each round-trip of the wave, with a duration of $\tau = 2l/c$, where l is the resonator length and c the speed of sound. All the variables can thus be discretized, x_n meaning the value of a variable x at time $n\tau$.

The behaviour of the whole instrument then can be described in a single iterative equation:

$$x_n = G\left(x_{n-1}, \gamma\right). \quad (3)$$

Function G can be obtained by replacing $p(t)$ and $u(t)$ in function F with Eq. (2). An explicit formulation for G is given by Taillard *et al.* [6], for $\zeta < 1$. Fig. 1(b) shows that the change from coordinates (p, u) to (x, y) can be performed graphically as a mirror about the axis $p = 0$ and a 45° rotation about the origin. Like F, G also depends on the control parameters γ and ζ. To keep the notation simple, the parameters will be omitted when constant. γ will be included as an argument to the function when it varies with time.

In most works on the clarinet, functions F and G are studied in a static-parameter regime, referring to a case where the instrument is blown at a constant pressure with a constant force applied on the lip. This article focuses on a case where the mouth pressure γ varies over time, a situation is referred to hereafter as dynamic-parameter regime, or simply dynamic regime. The graphics of Fig. 1(b) thus change over time.

2.2 Invariant manifolds and non-oscillating solutions

In a static-parameter regime, there is a value of $\gamma = \gamma_{st}$ establishing the transition between non-oscillating and oscillating solutions. This is called

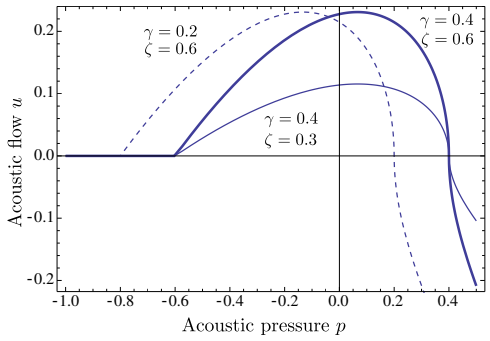

(a) F function

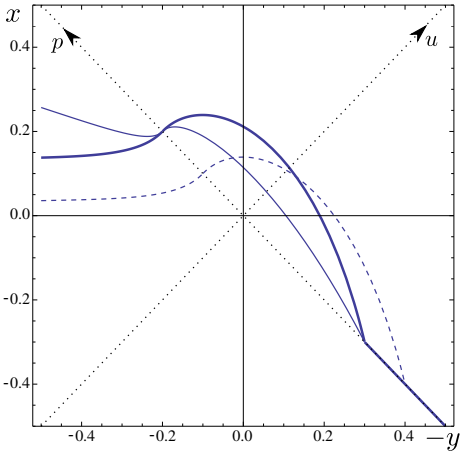

(b) G function

Figure 1: Non-linear characteristics in $u = F(p)$ representation (a) and $x = G(y)$ representation (b) for 3 different parameter values

the *static oscillation threshold*. Above this value, the clarinet system can oscillate, and will indeed oscillate for most initial values x_0. However, for particular sets of initial conditions (in the scope of this paper sets of γ_0 and x_0), the solution is non-oscillating. These sets correspond to the "invariant manifolds". If γ does not vary with time, the invariant manifold is called a fixed point, as the variable x will remain constant ($x = x_0$). The fixed point x^* can be found by solving:

$$x^* = G\left(x^*\right). \quad (4)$$

[1] x and y are usually written respectively as p^+ and p^-. The latter form is used in this article for conciseness.

x^* is a function of γ, $x^* = x^*(\gamma)$.

When γ varies with time, the invariant manifold cannot correspond to a single fixed point, but is also time-dependent, corresponding to an "invariant curve". Perhaps surprisingly, it is not the set of values $x^*(\gamma_n)$. The invariant curve is defined as the set of values $(x,\ \gamma)$ such that during the planned time-variation of γ, this set of values will always be followed, independently of the particular value the system is initiated in. The following equation is a defining condition for this curve:

$$\phi_\epsilon(\gamma) = G\left(\phi_\epsilon(\gamma - \epsilon), \gamma\right). \tag{5}$$

A method for calculating the invariant curve for the clarinet system is given in a previous article [13]. In appendix B simpler expressions for the invariant curve are given by using the characteristic curve expressed as $u = F(p)$ instead of function G. The invariant curve depends on how the parameter γ varies in time, i. e., it is different for different rates of variation of γ (different ϵ values).

2.3 Local stability of non-oscillating solutions

In both static and dynamic cases, the non-oscillating solutions can be either stable or unstable, depending on the behaviour of the system initialized close to the invariant manifold.

If initialized with a value x_0 close to a stable invariant manifold, the state variable x will approach it exponentially. Conversely, the state variable is repelled exponentially by an unstable manifold while in its vicinity. The distance to a fixed point (in a static-parameter case and while x_n is sufficiently close to the fixed point) is an exponential function of time (expressed as iteration number n) [18]:

$$x_n - x^* \approx (x_0 - x^*)\left[G'(x^*)\right]^n. \tag{6}$$

where $G'(x^*)$ is the derivative of the iterative function at the fixed point. When this value exceeds 1, the fixed point is unstable and the oscillation grows. Due to the non-linear nature of the system, the oscillation cannot grow forever, of course, and it stabilises in a periodic solution.

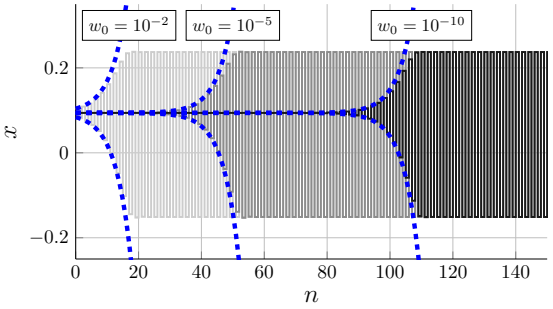

Figure 2: Time evolution of the outgoing pressure x, solution of Eq. (3) for different values of its initial value $x_0 = x^* + w_0$. From left to right: $w_0 = 0.01$ (——), $w_0 = 10^{-5}$ (——) and $w_0 = 10^{-10}$ (——). (- - -) Exponential envelope deduced from the function (6). The following parameters are used: $\gamma = 0.42$ (constant) and $\zeta = 0.5$.

In a static-parameter context, the oscillation would eventually stabilise in an oscillatory regime between values given by the 2-branch part of the static bifurcation diagram (an extensive discussion is given by Taillard *et al.* [6]).

For time-varying parameters, the evolution of the system can be interpreted as a dynamic bifurcation diagram. In this case, it is observed that the system still follows closely the invariant curve ϕ_ϵ even after it becomes unstable (see for instance Fig. 3). Eventually an oscillation appears at a value of mouth pressure much higher than the static oscillation threshold, so that we speak of a *bifurcation delay*. The new threshold is called the *dynamic oscillation threshold*. Above this threshold, a periodic regime is established whose amplitude is given approximately by the 2-branch part of the static bifurcation diagram.

The article focuses on providing the necessary elements to calculate the amplitude envelopes in different conditions, including when the time-variation of a parameter abruptly changes rate.

2.4 Similarities and differences between static and dynamic parameter cases

The duration of the transient is mainly characterized by two aspects:

- The time constant of the exponential approach or departure from the invariant manifold, which is proportional to $\log\left(G'(x^*)\right)$, as shown by Eq. (6)
- the value of the initial condition of x, or how far it is from the invariant curve or the fixed point.

Figure 2 illustrates how, for a similar exponential time constant (and parameters that are constant in time), it is possible to obtain very different transient times by changing the value of the initial conditions.

These are important results for understanding the behaviour of the system in a situation where the parameters change. The differences in dynamic parameter contexts are:

- If the parameter starts increasing at a value below the static oscillation threshold, the system will first undergo an approach to the invariant curve, and only beyond this value will it start the departure phase. In fact the approach can be so dramatic that a visible oscillation is only observed far beyond the static threshold.
- The exponential time-constant varies throughout the growth of the parameter, but it is not simply given by $\log\left(G'(x^*(t))\right)$ at each time t.

In realistic experimental situations, however, stochastic fluctuations prevent the system from coming too close to the invariant curve in the approach phase, and this can reduce the bifurcation delay.

3 Envelopes for dynamic-parameter regimes

This section provides a method to describe the oscillation amplitude in the particular case of a clarinet model system in which the blowing pressure parameter increases with time at a small constant nondimensional rate $\epsilon \ll 1$:

$$\begin{cases} x_n = G\left(x_{n-1}, \gamma_n\right) & \text{(7a)} \\ \gamma_n = \epsilon n + \gamma_0. & \text{(7b)} \end{cases}$$

3.1 Unlimited precision (noiseless)

First, the case with an arbitrarily high precision is analysed. x_n is the state variable of the system described in section 2.1. With the knowledge of x_n and its previous value x_{n-1} all remaining variables of the system can be calculated. In [13] it is shown that during a significant part of a slow transient, x_n is close to the invariant curve $\phi_\epsilon(\gamma)$ described above.

As seen in the previous section, for a constant parameter, the envelope is well described by an exponential envelope (Eq. (6)), as long as the state variable x remains sufficiently close to the fixed point x^* so that function G is well approximated by its tangent line.

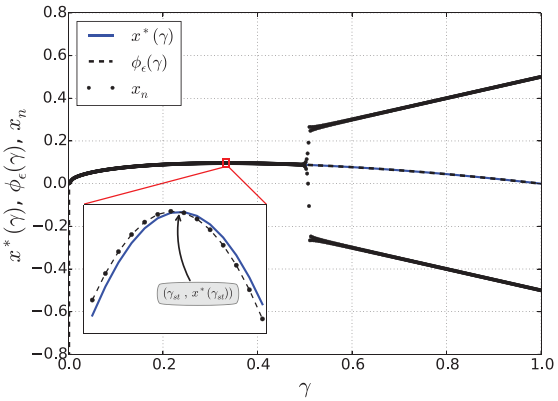

Figure 3: (black points) Numerical simulation of the system (7). (dashed black line) Invariant curve $\phi_\epsilon(\gamma)$. (blue line) Curve of fixed points $x^*(\gamma)$. $\zeta = 0.5$, $\epsilon = 10^{-3}$ and $\gamma_0 = 0$.

Fig. 3 suggests that when the parameter γ varies over time, x_n follows more closely the invariant curve than the curve of fixed points $(x^*(\gamma))$. Instead of

following the distance to the fixed point as in Eq. (6), a new variable w_n is therefore defined:

$$w_n = x_n - \phi_\epsilon(\gamma_n). \tag{8}$$

Note that, when the parameter is constant, the definition (8) reverts to $x - x^*$ of Eq. (6), as can be verified by substituting $\epsilon = 0$ in the perturbation approximation to ϕ_ϵ (see Appendix B, Eq. (30)).

For small amplitudes w_n, the function G in Eq. (7a) can be expanded as a first-order Taylor series around the invariant curve. The advantage of switching to this description is that future values of the oscillation amplitude $|w_n|$ can be approximated using a simple function $w(\gamma)$ relating to an initial iteration w_0:

$$|w_n| = w(\gamma_n) \approx |w_0| \exp\left(\frac{1}{\epsilon} \underbrace{\int_{\gamma_0+\epsilon}^{\gamma_n+\epsilon} \ln|G'\left(\phi_\epsilon(\gamma'-\epsilon),\gamma'\right)|\, d\gamma'}_{I(\gamma_n+\epsilon)-I(\gamma_0+\epsilon)} \right). \tag{9}$$

Eq. (9) is the equivalent to Eq. (6) for variable parameters (see [13] for details). Function I is defined by:

$$I(\gamma) = \int_{\gamma_{st}}^{\gamma} \ln|G'\left(\phi_\epsilon(\gamma'-\epsilon),\gamma'\right)|\, d\gamma'. \tag{10}$$

In the applications shown in this article, I is always used as a definite integral. As a consequence the integration constant, or one of the bounds of the integral I can be defined arbitrarily. γ_{st} is used in this article as a reference point close to the minimum amplitude, although for $\epsilon \neq 0$ the minimum is attained at a slightly lower pressure.

The discrete equivalent of Eq. (9) is:

$$\begin{aligned} |w_n| &= |w_0| \exp\left(\sum_{i=1}^{n} \ln|\partial_x G\left(\phi(\gamma_i-\epsilon),\gamma_i\right)| \right), \\ &= |w_0| \prod_{i=1}^{n} |\partial_x G\left(\phi(\gamma_i-\epsilon),\gamma_i\right)|. \end{aligned} \tag{11}$$

The "product form" (11) highlights that when the magnitude of G' is smaller than 1 in modulus, which happens before the static threshold γ_{st} is reached, x_n approaches the invariant curve. Beyond this threshold, x_n moves away from the invariant curve, but initially at a very slow pace, because the logarithm remains close to 0.

Although $I(\gamma)$ is not easy to calculate analytically, for small values of the increase rate ϵ, the derivative $G'\left(\phi_\epsilon(\gamma'-\epsilon),\gamma'\right)$ can be approximated by its value at the fixed point $G'\left(x^*(\gamma'),\gamma'\right)$, and the integral $I(\gamma)$ written in the form:

$$\tilde{I}(\gamma) = \int_{\gamma_{st}}^{\gamma} \ln|G'\left(x^*(\gamma'),\gamma'\right)|\, d\gamma'. \tag{12}$$

The error in $I(\gamma)$ committed in this approximation is observed to be smaller than ϵ (the difference between $I(\gamma)$ and $\tilde{I}(\gamma)$ in Fig. 4 is much smaller than ϵ).

For the clarinet model, the expressions involved in the calculation of the derivative G' are too complicated if function G is used in its explicit form. However, they can be obtained in a simple form (see Appendix B, Eq. (38)) from the definition of F in coordinates (p,u), providing simpler expressions for a numerical calculation of the integral. In the rest of this paper we use the approximate form (12).

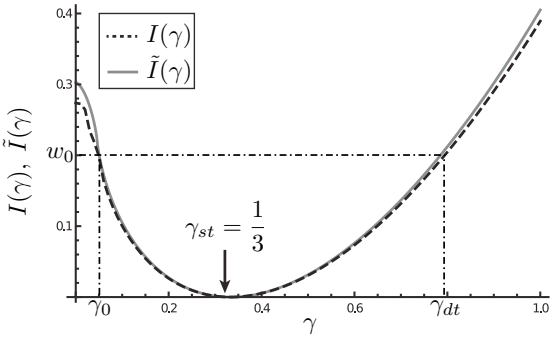

Figure 4: Integral $I(\gamma)$ calculated using Eq. (10) (dashed line) and approximately using Eq. (12) (solid line). $\zeta = 1/2$, $\epsilon = 1/20$.

The predicted amplitude $\widetilde{w}(\gamma)$ is calculated as a

distance to the invariant curve:

$$\widetilde{w}(\gamma) = |w_0| \exp\left(\frac{\tilde{I}(\gamma+\epsilon) - \tilde{I}(\gamma_0+\epsilon)}{\epsilon}\right). \quad (13)$$

At iteration n, $|w_n| \approx \widetilde{w}(\gamma_n)$. The graphic in Fig. 4 can be used to predict the qualitative behavior of the system: starting at a value γ_0, the distance to the invariant curve is a monotonic function of $\tilde{I}(\gamma+\epsilon)$. Whenever $\tilde{I}(\gamma+\epsilon) < \tilde{I}(\gamma_0+\epsilon)$, the amplitude is smaller than the starting value. Conversely, when $\tilde{I}(\gamma+\epsilon) > \tilde{I}(\gamma_0+\epsilon)$ the amplitude is higher. $\tilde{I}(\gamma+\epsilon) = \tilde{I}(\gamma_0+\epsilon)$ corresponds to the *dynamic oscillation threshold*, as defined in [13].

The curve described by Eq. (13) is often a good approximation of the envelope for most of the range of the growth parameter, except for large values of w_n, which typically arise in 2 situations:

- In the beginning of the transient, where the iterate x_0 can be far from the invariant curve, depending on the initial conditions. Note that the invariant curve usually diverges for small values of γ, so that even for reasonable values of x_0, the amplitude w_0 can be very large. The region where this curve diverges depends on ζ, but is usually well below the static threshold γ_{st} (see Appendix B.3).

- At the end of the transient, where x_n finally escapes from the invariant curve.

In practice these two situations can be avoided by carefully choosing the time interval of interest. For example, a few initial iterations may be calculated exactly using the recursive relation $x_n = G(x_{n-1})$ until they become sufficiently close to the invariant curve. In the end of the transient the envelope would not be valid for other reasons, in particular because the linear approximation in Eq. (13) is not valid (otherwise the envelope would grow indefinitely). The prediction $\widetilde{w_n}$ is valid until a few (3 or 4) iterations before the envelope starts stabilising in the oscillating branch of the bifurcation diagram.

3.2 Remarks on very low amplitudes

The curve $\widetilde{w}(\gamma)$ in Eq. (13) often reaches very small values if the value of ϵ is sufficiently small. As a quick example of application, consider a simulation started at a value of γ close to 0. For this case, Fig. 4 shows that the value of the amplitude at γ_{st} is $\widetilde{w}(\gamma_{st}) \simeq |w_0| \exp\left(-\frac{0.3}{\epsilon}\right)$. In this simulation, 0.3 is the difference between the minimum of I (at $\gamma \simeq \gamma_{st} = 1/3$) and the starting value of I. For $\epsilon = 1/100$, this means that the minimum amplitude will be $\exp(-30) \simeq 10^{-13}$. Reducing the increase rate by a factor of ten ($\epsilon = 1/1000$) brings the minimum amplitude down to the suprisingly low value of $\exp(-300) \simeq 5 \times 10^{-131}$. In general, the minimum amplitude reached by the system can be roughly calculated with:

$$w_{\min} = |w_0| \exp\left(\frac{\tilde{I}(\gamma_{st}) - \tilde{I}(\gamma_0)}{\epsilon}\right) \quad (14)$$

A few remarks are suggested by these extremely low values.

Firstly, extremely low values cannot be computed using ordinary machine precision. In this article, the calculations are performed with a *Python* library (*MPMath*) that simulates arbitrary precision in an ordinary machine. Fig. 5 shows how three different values of the precision produce very different envelopes. For certain values of γ the errors are many orders of magnitude higher than the precision of the calculations. Beyond a certain value of the precision, the envelope is not greatly affected, only producing "microscopic" errors, which are of the same magnitude as the precision. In practice, the precision a required to simulate the system should be higher than the minimum amplitude $w_{\min}$ reached by the system. This ensures that the difference between the simulation and the exact system never exceeds a, otherwise larger differences are expected because of the change in dynamic threshold.

Second, even if the simulations are performed using correct precision, the amplitudes w can only be seen relative to an accurately calculated invariant curve ϕ. The estimation of ϕ_ϵ requires a precision $a_{\text{IC}} < w_{\min}$ so that it can be used as an accurate reference for determining the amplitudes w.

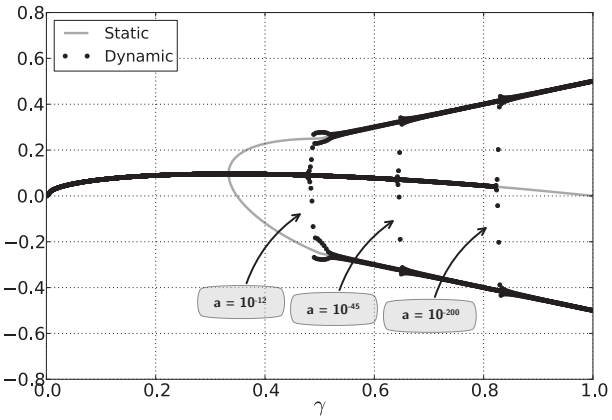

Figure 5: Static and dynamic bifurcation for $\zeta = 0.5$. Dynamic diagram is obtained with $\epsilon = 10^{-3}$ and $\gamma_0 = 0$, from numerical simulations performed with three different numerical precisions: $a = 10^{-12}$,$a = 10^{-45}$ and $a = 10^{-200}$.

In this paper, the invariant curve is calculated approximately using a perturbation series (see Appendix B), whose precision depends on the number of perturbation terms. Assuming that the perturbation terms $\phi_i(\gamma)$ all have the same magnitude (which as shown in Fig. 10 is true for $\gamma > 1/10$), the biggest influence in precision comes from the powers of ϵ that multiply each term in Eq. (30). Using this simple reasoning, a number of terms n is required for an invariant curve with precision a_{IC}:

$$\epsilon^n \approx a_{\mathrm{IC}} \quad \Longleftrightarrow \quad n \approx \frac{\log_{10}(a_{\mathrm{IC}})}{\log_{10}(\epsilon)}. \tag{15}$$

Returning to the previous example, for $\epsilon = 1/100$, $n = 7$ perturbation terms are required to observe correctly the envelope w at very low amplitudes, whereas for $\epsilon = 1/1000$ the number of terms is $n = 65$. However, even though the invariant curve requires a lengthy calculation in order to serve as a reference for the observation of w, a direct estimation $\tilde{w}$ can be obtained with a much cruder approximation of the invariant curve, as shown below.

Note that the previous argument is typically valid for high values of γ. For low values, some of the perturbation terms can reach values higher than 1, especially for high values of ζ. The argument seems valid in general above the static threshold (see appendix B.3 and Fig. 10).

In real systems, the problem of precision does not apply. However, experimental systems are very often affected by noise from different sources. The major source of noise in the clarinet is turbulence, which cannot be avoided even with a very precise control of the pressure. Noisy situations, as well as finite precision situations, can be analysed introducing a stochastic variable in the iterative system (Eq. (7))

3.3 Trajectory of the system affected by noise

If numerical simulations are run with a precision coarser than the w_{min} calculated through Eq. (14), the previous formulæ must be extended. The limited precision (i.e. below w_{min}) used in simulations is modelled as a stochastic variable (with a standard deviation of $\sigma = a$) in the system. This case is studied in [16]. A "squared average" trajectory $< w_n^2 >$ is described by:

$$< w_n^2 > \approx \underbrace{\widetilde{w}(\gamma_n)^2}_{A(\gamma_n)} + \underbrace{\frac{\sigma^2}{\epsilon}\int_{\gamma_0+\epsilon}^{\gamma_n+\epsilon}\left(\frac{\widetilde{w}(\gamma_n)}{\widetilde{w}(\gamma')}\right)^2 d\gamma'}_{B(\gamma_n)}. \tag{16}$$

The two terms of the right-hand side of Eq. (16) are functions of the parameter γ. The term labeled $A(\gamma)$ corresponds to the approximation of the trajectory in the absence of noise, the same as in Eq. (9). $B(\gamma)$ is the expected value of the additional distance to the invariant curve due to the presence of noise. In practice, when the noise level is sufficiently high or the precision low (relative to the estimation of Eq. (15)), only the term $B(\gamma)$ is relevant, i.e. the trajectory of the system is described by: $\sqrt{< w_n^2 >} \approx \sqrt{B(\gamma_n)}$ with

$$B(\gamma) = \frac{\sigma^2}{\epsilon}\int_{\gamma_0+\epsilon}^{\gamma+\epsilon}\left(\frac{w(\gamma)}{w(\gamma')}\right)^2 d\gamma'. \tag{17}$$

For ϵ sufficiently small, since $\tilde{I} > 0$ by definition and considering Eq. (13), it can be deduced that $\widetilde{w}(\gamma) \gg \widetilde{w}(\gamma')$ for γ' close to γ_{st} (keeping in mind that $\widetilde{w}$ depends exponentially on $\tilde{I}/\epsilon$ with ϵ small, in this article, and the minimum of I and w are close to γ_{st}) and w is negligible for all remaining values of γ'. This allows a simplification of the expression for $B(\gamma)$ as described below.

According to the shape of $\tilde{I}(\gamma)$ (see Fig. 4), a second-order Taylor expansion of $\tilde{I}(\gamma)$ around the static oscillation threshold γ_{st} is used to simplify its expression (for details, see Appendix C):

$$\tilde{I}(\gamma) \approx 3\sqrt{3}\frac{\zeta}{2}(\gamma - \gamma_{st})^2. \tag{18}$$

Using approximation (18), the expression of $B(\gamma)$ can be simplified to:

$$B(\gamma) = \sigma^2 \sqrt{\frac{\pi}{3\sqrt{3}\zeta\epsilon}} \exp\left(2\frac{\tilde{I}(\gamma+\epsilon)}{\epsilon}\right). \tag{19}$$

Details of the calculations of the simplified expression (19) are given in Appendix D. This amplitude $B(\gamma)$ does not depend on the starting amplitude w_0, and is also independent of the starting value of γ.

It is interesting to notice that according to (13), expression (19) can also be written:

$$B(\gamma) = \sigma^2 \sqrt{\frac{\pi}{3\sqrt{3}\zeta\epsilon}} \times \exp\left(2\frac{\tilde{I}(\gamma_0+\epsilon)}{\epsilon}\right)\left(\frac{w(\gamma)}{w_0}\right)^2. \tag{20}$$

In this form, Eq. (20) shows that, in the presence of noise and far beyond the static threshold, the envelope followed by the system has the same shape as without noise, but with a different amplitude, i.e in this case we have:

$$\sqrt{< w_n^2 >} \approx \sqrt{B(\gamma_n)} \approx K\ w(\gamma_n), \tag{21}$$

where K is a constant deduced from Eq. (20).

As a remark, a different calculation with similar objectives is made in a previous article [16] to determine the dynamic thresholds in presence of noise. The approximation (18) was used formally to integrate $\tilde{I}(\gamma_n + \epsilon)$ in Eq. (19). The result is an explicit expression for $B(\gamma)$, and therefore of the dynamic oscillation threshold. Here, $\tilde{I}(\gamma_n + \epsilon)$ is numerically integrated, keeping its precise expression given by Eq. (12). This leads to a better estimation of the envelope, but that envelope does not have an analytic expression.

4 Interrupted variation of the mouth pressure parameter

This section describes the behaviour of the system for an example profile consisting of a limited linear growth of the parameter at a constant rate ϵ followed by a constant value γ_M for an indefinite period of time. The parameter is therefore formally defined as:

$$\gamma_n = \begin{cases} \epsilon n + \gamma_0 \text{ if } n \leq M & \text{(22a)} \\ \gamma_M \text{ if } n > M. & \text{(22b)} \end{cases}$$

Due to the change in increase rate at $n = M$ the growth phase and the static phase are studied independently. An amplitude envelope $\tilde{w}^-(\gamma)$ is computed for the growth phase and another $\tilde{w}^+(\gamma)$ for the static phase. The two envelopes are connected at $n = M$ since the initial value $\tilde{w}^+(\gamma_M)$ is deduced from $\tilde{w}^-(\gamma_M)$. The method is described in the next sections and summarised in Fig. 6.

4.1 Amplitude envelope of the growing phase: w^-

As explained in section 3, the first few (N_{lin}) iterations must usually be performed manually. These correspond to an "approach phase" that brings the system close enough to the invariant curve so that the assumption of linearity is valid.

At iteration N_{lin} the state of the system is given

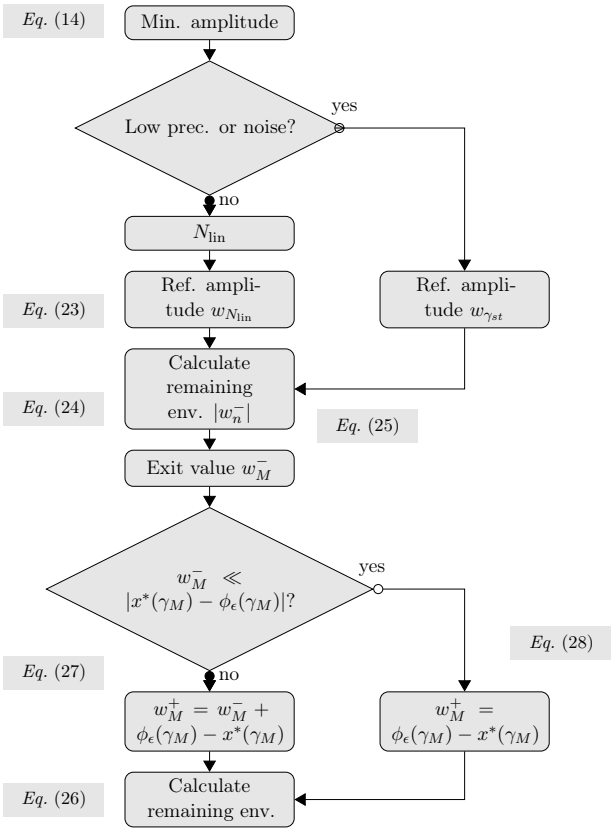

Figure 6: Algorithm for determination of the envelope.

by:

$$\begin{aligned} n &= N_{\rm lin} \\ x_{N_{\rm lin}} &= G^{N_{\rm lin}}(x_0) = \underbrace{G \circ G \circ \ldots \circ G}_{N_{\rm lin}\,\text{times}}(x_0) \\ \gamma_{N_{\rm lin}} &= \gamma_0 + N_{\rm lin}\epsilon \\ w^+_{N_{\rm lin}} &= x_{N_{\rm lin}} - \phi_\epsilon(\gamma_{N_{\rm lin}}) \end{aligned} \quad (23)$$

The number of iterations required for the approach phase depends on the starting value of γ and the increase rate ϵ. In practice the state of the system is simulated iteratively until it reaches an amplitude $w_n < \epsilon$.

A complication to this view arises when γ goes through a superstable point γ_{ss} defined by $G'(x^*(\gamma_{ss}), \gamma_{ss}) = 0$. At this point the iterations can approach arbitrarily the invariant curve. Although this situation can be analysed under some simplifying assumptions, this is not done in this article, and the reader is referred to Baesens [14] for a detailed description of this case or to Bergeot [19] in the context of the clarinet. A simple way of circumventing this problem is to force $N_{\rm lin}$ to bring γ beyond the super-stable point.

A few explicit iterations (usually less than 5) allow the calculation of the amplitude $w(\gamma_{N_{\rm lin}})$. Iteration $n = N_{\rm lin}$ is used as a safe starting point for the analytic determination of the envelope.

$$\widetilde{w}^-(\gamma) = \left|w^-_{N_{\rm lin}}\right| \times \exp\left(\frac{\tilde{I}(\gamma+\epsilon) - \tilde{I}(\gamma_{N_{\rm lin}}+\epsilon)}{\epsilon}\right). \quad (24)$$

When the simulations are performed with a lower precision than that required for simulating the exact system (see Eq. (15)), the initial value γ_0 does not affect the growth of oscillations. In this case, an average squared amplitude is given by Eq. (19) starting from γ_{st}. Therefore, the envelope is given by:

$$\widetilde{w}^-(\gamma) = \sigma\left(\frac{\pi}{3\sqrt{3}\zeta\epsilon}\right)^{1/4} \exp\left(\frac{\tilde{I}(\gamma+\epsilon)}{\epsilon}\right). \quad (25)$$

This approximation is valid for $\gamma > \gamma_{st}$, which is the usual region of interest. Below γ_{st} the oscillations are mostly random, with an average level that remains close to the standard deviation of the stochastic perturbation σ.

4.2 Amplitude envelope of the static phase: w^+

At $n = M$, γ becomes constant and the oscillation undergoes an exponential growth (provided that $\gamma_M > \gamma_{st}$), given by Eq. (6) where the initial value w_0 is replaced by the value w_M^+ deduced from the previous study of the growing phase:

$$\widetilde{w}^+_n = \left|w^+_M \left[G'(x^*(\gamma_M), \gamma_M)\right]^{(n-M)}\right|. \quad (26)$$

The starting amplitude w_M^+ for the static phase is given by continuity of x:

$$w_M^+ = \widetilde{w}^-(\gamma_M) + \phi_\epsilon(\gamma_M) - x^*(\gamma_M). \tag{27}$$

due to the change in invariant manifold from the invariant curve $\phi_\epsilon(\gamma)$ to $x^*(\gamma_M)$.

As a remark, when the amplitude $\widetilde{w}^-(\gamma_M)$ is sufficiently small (i. e. $\widetilde{w}^-(\gamma_M) \ll |x^*(\gamma_M) - \phi_\epsilon(\gamma_M)|$), the starting amplitude can be given simply by the difference between the invariant curve and the curve of fixed points:

$$w_M^+ = \phi_\epsilon(\gamma_M) - x^*(\gamma_M). \tag{28}$$

In such a situation, the transient time is roughly given by the time until the slope discontinuity in the blowing pressure profile, plus a delay corresponding to the time needed for the oscillations to grow from w_M^+ (independently of w_M^-) to the final amplitude. Since the starting amplitude and the exponential coefficient ($G'(x^*)$ in Eq. (6)) are independent of the slope of the growth phase, so is the duration of the transient resulting from the interruption in the growth. This matches observations on real instruments blown artificially [11].

In any case, the oscillation usually starts very close to the fixed point $x^*(\gamma_M)$. This ensures that the linear approximation is valid on a large part of the transient (see Fig. 2).

5 Examples

A few examples of simulations are presented in this section, together with predictions based on the previous sections, and their limitations. The "actual envelopes" corresponding to the absolute distance between the iterated values and the invariant curve are plotted together with the estimation of the envelopes (Eq. (16)). In examples presented in sections 5.1 and 5.2 the numerical precision is higher than the minimum amplitude reached by the system (Eq. (14)). The effect of introducing a stochastic variable in the system, which plays a similar role as performing simulations with low precision [16], is shown in the example of section 5.3.

5.1 Interruption below dynamic oscillation threshold

In Fig. 7, the increase in mouth pressure γ is stopped at a relatively small value of the parameter. In consequence, the amplitude of the oscillations is considerably smaller when the increase is interrupted. A jump in the relative amplitude is observed when $\gamma = \gamma_M$, in a logarithmic plot (see Fig. 7(b)). This jump arises because w is the distance to the invariant curve ϕ_ϵ before γ_M and to the fixed point x^* after.

In this example, 6 iterations (N_{lin}) are used to reach the linear approximation. Moreover $\widetilde{w}^-(\gamma_M) \ll |x^*(\gamma_M) - \phi_\epsilon(\gamma_M)|$, so that the starting amplitude for the constant parameter phase (w_M^+) is deduced from Eq. (28). The envelope is then computed following the method described above (see Fig. 6).

Fig. 7(b) also shows that the prediction is slightly in advance relative to the actual envelope. The reason is that $\tilde{I}(\gamma)$ is calculated using a severe approximation $\phi_\epsilon(\gamma - \epsilon) \approx x^*(\gamma)$ (see Eq. (12)). For small values of ϵ the approximation is satisfactory. The advantage of using this approximation is that a single curve $\tilde{I}(\gamma)$ can be used for any small value of the growth rate.

5.2 Interruption near the dynamic oscillation threshold

In Fig. 8, γ reaches a higher stable value. This results in higher values of amplitude w_n when the parameter stops increasing.

The envelopes during the growing phase are estimated using the same method as in the previous example. At iteration M, since the system is estimated to have an amplitude that is higher than the difference $|\phi(\gamma) - x^*(\gamma_M)|$, the new amplitude w_M^+ is the distance to the invariant curve of the growing phase $\widetilde{w}^-(\gamma_M)$. The remaining envelope is the exponential $w_M^+ \exp|G'(x^*(\gamma_M), \gamma_M)|$, as in the example above.

The biggest difficulty in estimating the amplitude of the static phase arises when the amplitude $\widetilde{w}^-(\gamma_M)$ is similar to $|\phi(\gamma) - x^*(\gamma_M)|$. In this case, the iterate at $n = M$ can be either very close to the fixed point curve or at twice the distance between the two

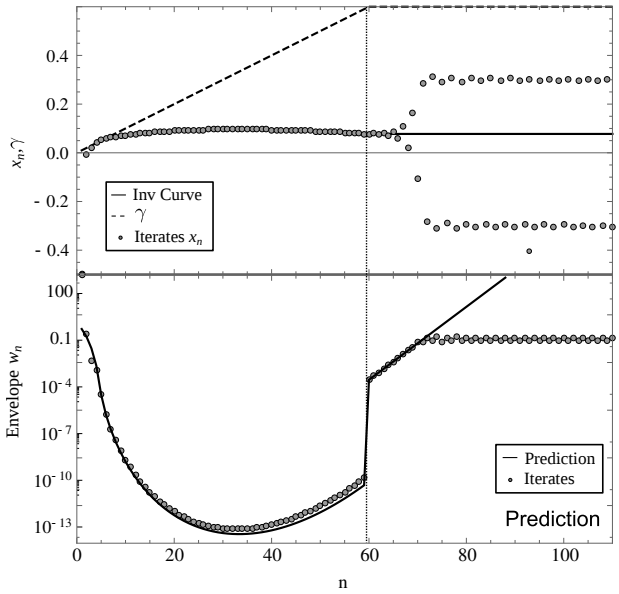

Figure 7: Simulation of the system in Eq. (5) with unlimited precision. The invariant curve (Eq. (29)) is calculated with 8 perturbation terms and envelope predictions given by Eq. (13). $\epsilon = 0.01$, $\zeta = 1/2$, $\gamma_M = 0.6$, $\gamma_0 = 1/10000$, $x_0 = 0.5$.

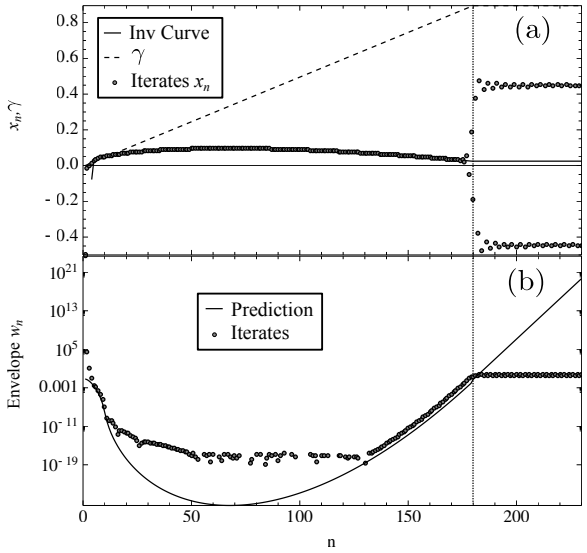

Figure 8: Simulation of the system in Eq. (5) with unlimited precision. The invariant curve (Eq. (29)) is calculated with 8 perturbation terms and envelope predictions given by Eq. (13). $\epsilon = .005$, $\zeta = 1/2$, $\gamma_M = 0.9$, $x_0 = 0.5$, $\gamma_0 = 1/10000$.

reference curves, which will imply very different amplitudes for the static phase.

Finally, in Fig. 8(b), the jump in relative amplitude at the beginning of the static phase exists but it is not clearly visible because the amplitude of the oscillation at $\gamma = \gamma_n$ is large compared with the case shown in the previous example (see Fig. 7(b)).

The disagreement between the iterates and the prediction for $10 < n < 130$ may appear to suggest that the prediction is not good here, whereas in fact it is the "actual envelope" that is incorrect. This is due to an inaccurate determination of the invariant curve. In fact, the number of terms needed for the invariant curve (Eq. (15)) makes its analytical computation too complicated. This situation is thus different from the numerical precision problem outlined in Fig. 5, where the iterates are in some cases very different from those of the ideal system simulated with infinite precision due to the shift in dynamic threshold. The prediction is valid for most of the simulation between $n = 4$ and $n = 160$, and it matches the envelope whenever the invariant curve is valid (in particular above $n = 130$). This shows that the envelope and the dynamic threshold can be fairly well predicted, even with an inaccurate approximation.

5.3 Simulations with noise

In the example of Fig. 9, the simulation is performed adding a stochastic variable to γ_n with a uniform probability distribution having a standard deviation $\sigma = 10^{-4}$. This is roughly equivalent to a simulation without noise but with a numerical precision fixed to 4 significant digits (i.e. $a = 10^{-4}$) [16].

The sequence $B(\gamma_n)$ (Eq. (19)) is calculated based on this value of σ, and its square-root plotted as the envelope prediction. The prediction is valid for $\gamma > \gamma_{st} = 1/3$, where $B(\gamma_n)$ reaches its minimum value. The departure of the oscillations occurs earlier when compared to the case without noise. When $\gamma < \gamma_{\rm st}$

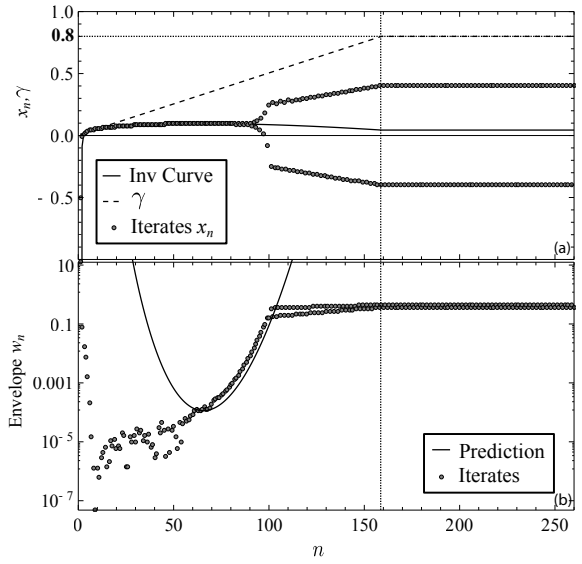

Figure 9: Simulation of the system in Eq. (3) with linearly increasing γ and added noise. Invariant curve (Eq. (29)) and envelope predictions given by Eq. (21). Unlimited precision, $\epsilon = .01$, $\zeta = 1/2$, $x_0 = 0.5$, $\gamma_0 = 1/10$, $\sigma = 10^{-4}$.

the amplitude is roughly that of the noise, because the noise is added at each new iteration to a value smaller that of the non-linear function applied to the previous iteration.

Because of the reduction in the bifurcation delay, the oscillations are seen to depart much earlier than the cessation of the increase of the parameter γ. After the end of the exponential increase in amplitude, the envelope increases with the parameter, following the two-state oscillation given by the static bifurcation diagram.

A discontinuity similar to that observed in figure 7 can arise also in noisy conditions. However, because the envelope curve $w(\gamma)$ multiplies a bigger value at γ_{st}, the discontinuity is seen only for smaller values of γ_M.

Due to the random nature of the system, the prediction should not be interpreted as an approximation to the exact envelope, but rather as the envelope followed on average by a series of runs of the simulation. In fact, in this case, for a series of runs with different noise samples, the actual envelope was seen to shift towards the right or the left by about 4 iterations.

6 Discussion

The method can in principle be extended to include frequency independent losses [8], although this may be hard to acheive analitically. The invariant curve cannot be calculated directly from the simple expression of F, as in Appendix B, requiring the use of the much more complicated expressions of G and its derivatives. More complex models of clarinets with frequency dependent losses are known to give rise to long attack transients with similar envelope shapes [12], and the envelope estimation used in the present article may be similar in models with small dispersion in the reflection function [20].

When the mouth pressure grows linearly over time, the logarithm of the amplitude is proportional to a predetermined curve, which we call $I(\gamma)$. The proportionality factor depends on the inverse of the growth rate ϵ, whereas the offset depends on one of these two factors:

- the initial amplitude (starting distance to the invariant curve), when the precision is high enough (see Eq. (13)) or
- the stochastic level σ when the simulation is imprecise or the system is noisy (Eq. (21)).

A stop in the linear growth of the mouth pressure may occur while the system is still oscillating with low amplitude. In this case, when the pressure stops increasing, the oscillation resumes exponentially from a higher amplitude, which is given by the distance between the invariant curve and the fixed point at the particular value of the mouth pressure. A discontinuity in the amplitude envelope is observed if before the mouth pressure stops increasing while the amplitude was still at a value lower than the distance between the invariant curve and the fixed point.

Bifurcation delay has also been observed in a real instrument. So far it has been hard to relate the amplitude envelope to the value of the mouth pressure. In interrupted ramps of the mouth pressure however, the oscillations seem to be triggered close to the inflection point of the blowing pressure [11]. In this case, an exponential amplitude growth then resumes. This is as expected for low values of γ_M, as shown in the example in section 5.1.

The values of γ at the start of the oscillation depend on the rate of growth of the mouth pressure, an indication that the system is determined by the stochastic fluctuations in the mouth pressure.

For a constantly increasing parameter, the *dynamic oscillation threshold* γ_{dt} [13, 16] gives the approximate value of the mouth pressure parameter for which an audible sound appears, or in other terms, the distance from the invariant w curve becomes "macroscopic". When the linear growth of the mouth pressure is suddenly stopped at $n = M$ and then kept constant at a value γ_M, two situations must be distinguished:

- $\gamma_M < \gamma_{dt}$: a growing exponential envelope starts at $\gamma = \gamma_M$ with a fixed starting amplitude, which only depends on the value of γ_M (see section 5.1). Audible sound occurs at a fixed time interval from the stop in pressure increase;
- $\gamma_M > \gamma_{dt}$: the audible ("macroscopic") sound begins at $\gamma = \gamma_{dt}$ (see sections 5.2 and 5.3).

In most practical cases the latter situation is more common: because of the limited precision or noise, γ_{dt} is effectively reduced to values that are much closer to the static threshold.

7 Conclusion

This work shows that the amplitude envelope produced with a regular increase of blowing pressure in a simplified clarinet system can be described reasonably well by the use of a single function $I(\gamma)$ that is a characteristic of the system. This function can be used in exact and "noisy" cases to describe the envelope beyond the static threshold γ_{st}.

When the pressure increase is interrupted, the exponential envelope corresponding to the transient of a static-parameter case can be matched with the one corresponding to growing pressures. In many practical cases, when the interruption occurs at sufficiently low values of the blowing pressure, this corresponds to a fixed starting amplitude so that the transient time measured from the interruption is roughly independent of the previous history of the system.

These conclusions show some dramatic effects of the stabilisation of the mouth pressure that are due to the discontinuity in derivative.

In summary, a sudden cessation in the increase in-mouth pressure can have a large impact in the initial transient of the clarinet if it appears at a low enough value of mouth pressure. A preliminary comparison with a smoother stabilisation profiles [21] suggests that smoother profiles give rise to slower transients. However, because of the simple mathematic expressions used for the profiles, they are not easy to compare to the piecewise linear profiles shown in this article.

Acknowledgement

This work is part of the research project SDNS-AIMV "Systèmes Dynamiques Non-Stationnaires - Application aux Instruments à Vent" (ANR-09-RPDOC-022-01) financed by the *Agence Nationale de la Recherche*. The authors thank Prof. Joe Wolfe for useful suggestions and proof reading.

A Table of notation

$p(t)$	non-dimensional pressure
$u(t)$	non-dimensional flow
γ	mouth pressure parameter
ζ	embouchure parameter
$G(x)$	iterative function
x_n	outgoing wave (also p_n^+)
$x^*(\gamma)$	fixed points of the function $G(x)$; same as $\phi_{\epsilon=0}$
$\phi_\epsilon(\gamma)$	invariant curve (depends on ϵ)
$I_\epsilon(\gamma)$	"Base curve" used in calculations of ϕ and w (depends on ϵ)
$\widetilde{I}(\gamma)$	Approximation to the "base curve" I, independent of ϵ
w_n	difference between a simulated x_n and ϕ
$\widetilde{w}(\gamma_n)$ or $\widetilde{w}_n$	prediction of w_n
ϵ	increase rate of the parameter γ
σ	level of the white noise
a	numerical precision used in calculations
$A(\gamma)$	deterministic contribution to w
$B(\gamma)$	stochastic contribution to w
γ_{st}	static oscillation threshold
γ_{dt}	dynamic oscillation threshold
M	iteration number at which γ stops increasing
γ_M	target mouth pressure (γ)

B Perturbation methods for the invariant curve

This appendix presents a perturbation method to calculate the invariant curve, using only expressions of function $u = F(p)$ (see Eq. (1)). This has the advantage of producing much simpler expressions than using function $x = G(-y)$ (Eq. (3)). Higher order terms are needed only when determining w_n from a simulation. For all other purposes used in this article, the first order term is usually sufficient.

B.1 Generic forms of the invariant curve.

The invariant curve satisfies the following equation:

$$\phi_\epsilon(\gamma) = G\left(\phi_\epsilon(\gamma-\epsilon),\gamma\right). \tag{29}$$

The perturbation to order K consists in expressing ϕ_ϵ as a series of terms depending on powers of ϵ (the perturbation):

$$\phi(\gamma) = \sum_{i=0}^{K} \epsilon^i \phi_i(\gamma) + o(\epsilon^{K+1}) \tag{30}$$

Both ϕ_ϵ and G are developed in a power series, ϕ_ϵ around $\gamma$and G around the first term ϕ_0

The right-hand side of Eq. (29) is then, to 2nd order:

$$\begin{aligned} G\left(\phi_\epsilon(\gamma-\epsilon),\gamma\right) = {} & G\left(\phi_0(\gamma),\gamma\right) + \\ & G'\left(\phi_0(\gamma,\gamma)\left(\phi_1(\gamma)-\phi_0'(\gamma)\right)\right)\epsilon + \\ & \left(\frac{1}{2}\left(\phi_1(\gamma)-\phi_0'(\gamma)\right)\right) G''\left(\phi_0(\gamma,\gamma)+\right. \\ & G'\left(\phi_0(\gamma,\gamma)\left(\phi_2(\gamma)-\phi_1'(\gamma)-\frac{1}{2}\phi_0''(\gamma)\right)\right) + \\ & O(\epsilon^3). \end{aligned} \tag{31}$$

By equating expression (30) on the left-hand side and (31), it is possible to isolate terms on each power of ϵ, and extract expressions for each of the functions ϕ_i.The first term is nothing but the definition of the fixed point:

$$\phi_0(\gamma) = G\left(\phi_0(\gamma)\right). \tag{32}$$

Each of the higher order terms is obtained from lower-order ones:

$$\phi_1 = \frac{G'\left(\phi_0\right)\phi_0'}{G'\left(\phi_0\right)-1} \tag{33}$$

$$\phi_2 = \frac{G'\left(\phi_0\right)\left(2\phi_1\phi_0' - \phi_1^2 - \phi_0'^2\right)}{2\left(G'\left(\phi_0\right)-1\right)} + \tag{34}$$

$$\frac{G''\left(\phi_0\right)\left(2\phi_1-\phi_0''\right)}{2\left(G'\left(\phi_0\right)-1\right)} \tag{35}$$

$\cdots$

All functions and derivatives of the functions ϕ_i are taken at γ. As expected, all the derivatives of G are taken at the fixed point ϕ_0, and this remains true for higher-order terms too.

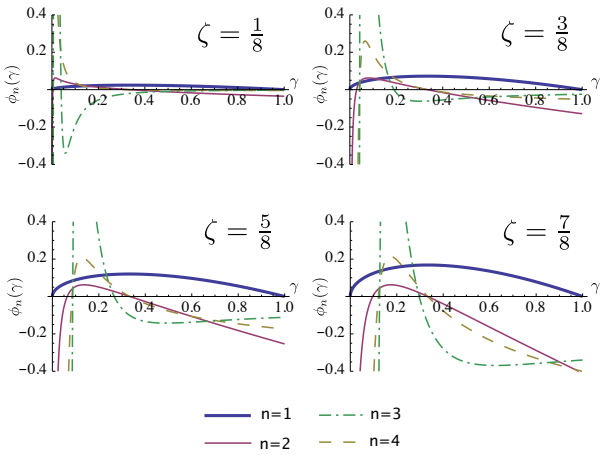

Figure 10: First four terms of the perturbation approximation to the invariant curve as a function of γ for four different values of ζ.

B.2 Derivatives of G at the fixed point.

Derivatives of function G, as given by Taillard [6] are hard to calculate, as the expressions are complex. However, the derivatives of G are related to those of function F. $y = G(x)$ can be defined as a parametric curve (with parameter p) as the locus of points:

$$x(p) = -\frac{1}{2}\left(p - F(p)\right), \tag{36}$$

$$y(p) = \frac{1}{2}\left(p + F(p)\right). \tag{37}$$

The derivative of the curve $y = G(x)$ is:

$$G' = \frac{\frac{\partial y}{\partial p}}{\frac{\partial x}{\partial p}} = \frac{F'+1}{F'-1} = \frac{-2\sqrt{\gamma - p} + \zeta\left(3(p-\gamma)+1\right)}{2\sqrt{\gamma - p} + \zeta\left(3(p-\gamma)+1\right)}. \tag{38}$$

All higher order derivatives can be calculated iteratively:

$$G^{(n)} = \frac{\frac{\partial G^{(n-1)}}{\partial p}}{\frac{\partial x}{\partial p}}. \tag{39}$$

For instance the second derivative is:

$$G'' = -\frac{4F''}{(F'-1)^3} = -\frac{8\zeta(-3\gamma+3p-1)}{\left(2\sqrt{\gamma-p}+\zeta\left(3(p-\gamma)+1\right)\right)^3}. \tag{40}$$

In general these formulas are not of much use because they are functions of p instead of x. However, it can be proved that the fixed point of G corresponds to $p = 0$ (the line $y = x$ corresponds to the axis u), so that:

$$G'(\phi_0(\gamma)) = \frac{-2\sqrt{\gamma} + (1-3\gamma)\zeta}{2\sqrt{\gamma} + (1-3\gamma)\zeta}, \tag{41}$$

and

$$G''(\phi_0(\gamma)) = -\frac{8\zeta(3\gamma+1)}{\left(2\sqrt{\gamma} + (1-3\gamma)\zeta\right)^3}. \tag{42}$$

etc.

B.3 Perturbation terms.

From Eqs (33) and (35), the first perturbation terms can be written:

$$\phi_0(\gamma) = \frac{\zeta}{2}(1-\gamma)\sqrt{\gamma}, \tag{43}$$

$$\phi_1(\gamma) = \frac{(1-3\gamma)\zeta\left((3\gamma-1)\zeta + 2\sqrt{\gamma}\right)}{16\gamma}, \tag{44}$$

$$\phi_2(\gamma) = -\frac{\left(9\gamma^2-1\right)\zeta^2\left(5\zeta(3\gamma-1)+8\sqrt{\gamma}\right)}{256\gamma^{5/2}} \tag{45}$$

The first perturbation terms (ϕ_i for $i = 1$ to 4) are represented graphically in Fig. 10.

C Approximated expression of $\tilde{I}(\gamma)$

According to the shape of $\tilde{I}(\gamma)$, the second-order Taylor expansion of $\tilde{I}(\gamma)$ around the static oscillation threshold γ_{st} is:

$$\tilde{I}(\gamma) \approx \tilde{I}(\gamma_{st}) + (\gamma - \gamma_{st})\tilde{I}'(\gamma_{st}) + \frac{(\gamma - \gamma_{st})^2}{2}\tilde{I}''(\gamma_{st}). \quad (46)$$

Through Eq. (12), by definition, we have $\tilde{I}(\gamma_{st}) = 0$. Since $\tilde{I}(\gamma)$ is the integral of a known function, at the static threshold, the expression of the first and the second derivatives of $\tilde{I}(\gamma)$ are:

$$\tilde{I}'(\gamma_{st}) = \ln|G'(x^*(\gamma_{st}), \gamma_{st})| = 0, \quad (47)$$

$$\tilde{I}''(\gamma_{st}) = \left(\frac{d}{d\gamma}\ln|G'(x^*(\gamma), \gamma)|\right)_{\gamma=\gamma_{st}}. \quad (48)$$

Eq. (48) can be calculated explicitly from the expression of $G'(x^*(\gamma), \gamma)$, given by Eq. (41). The resulting expression estimated in $\gamma = \gamma_{st}$. After calculation we obtain $\tilde{I}''(\gamma_{st}) = 3\sqrt{3}\zeta$, yielding:

$$\tilde{I}(\gamma) \approx 3\sqrt{3}\frac{\zeta}{2}(\gamma - \gamma_{st})^2, \quad (49)$$

with a quadratic approximation close to γ_{st}.

D Details of the calculation of the simplified expression of $B(\gamma)$

Using Eq. (13), Eq. (17) is developed,

$$B(\gamma) = \frac{\sigma^2}{\epsilon}\int_{\gamma_0+\epsilon}^{\gamma+\epsilon}\left(\frac{\widetilde{w}(\gamma)}{\widetilde{w}(\gamma')}\right)^2 d\gamma' = \frac{\sigma^2}{\epsilon}\exp\left(2\frac{\tilde{I}(\gamma+\epsilon)}{\epsilon}\right) \times \int_{\gamma_0+\epsilon}^{\gamma+\epsilon}\exp\left[2\left(\frac{-\tilde{I}(\gamma'+\epsilon)}{\epsilon}\right)\right]d\gamma', \quad (50)$$

and replacing $\tilde{I}(\gamma)$ by its expression given by Eq. (18), the term $B(\gamma)$ is approximated by:

$$B(\gamma) = \frac{\sigma^2}{\epsilon}\exp\left(2\frac{\tilde{I}(\gamma+\epsilon)}{\epsilon}\right) \int_{\gamma_0+\epsilon}^{\gamma+\epsilon}\exp\left(-\frac{3\sqrt{3}\zeta}{\epsilon}\left(\gamma'+\epsilon-\gamma_{st}\right)^2\right)d\gamma', \quad (51)$$

Eq. (51) can be formally integrated using the error function $\mathrm{erf}(x)$ [22]:

$$B_n = \frac{\sigma^2}{\epsilon}\exp\left(2\frac{\tilde{I}(\gamma+\epsilon)}{\epsilon}\right)\frac{1}{2}\sqrt{\frac{\pi\epsilon}{3\sqrt{3}\zeta}} \times \left[\mathrm{erf}\left(\sqrt{\frac{3\sqrt{3}\zeta}{\epsilon}}\left(\gamma'+\epsilon-\gamma_{st}\right)\right)\right]_{\gamma_0+\epsilon}^{\gamma+\epsilon}. \quad (52)$$

The term in square brackets in Eq. (52) can often be approximated to the values of the error function far from γ_{st}, respectively -1 and 1, allowing to write:

$$\left[\mathrm{erf}\left(\sqrt{\frac{3\sqrt{3}\zeta}{\epsilon}}\left(\gamma'+\epsilon-\gamma_{st}\right)\right)\right]_{\gamma_0+\epsilon}^{\gamma_n+\epsilon} \approx 2. \quad (53)$$

Finally, using Eq. (53), the expression of $B(\gamma)$ becomes:

$$B(\gamma) = \sigma^2\sqrt{\frac{\pi}{3\sqrt{3}\zeta\epsilon}}\exp\left(2\frac{\tilde{I}(\gamma_n+\epsilon)}{\epsilon}\right). \quad (54)$$

References

[1] M. E. McIntyre, R. T. Schumacher, J. Woodhouse: On the oscillations of musical instruments. J. Acoust. Soc. Am. **74** (Nov. 1983) 1325–1345.

[2] T. A. Wilson, G. S. Beavers: Operating modes of the clarinet. J. Acoust. Soc. Am. **56** (1974) 653–658.

[3] R. T. Schumacher: Ab initio calculations of the oscillations of a clarinet. Acustica **48** (1981) 71–85.

[4] S. Ollivier, J. P. Dalmont, J. Kergomard: Idealized models of reed woodwinds. part 2 : On the stability of two-step oscillations. Acta Acust. united Ac. **91** (2005) 166–179.

[5] J. Kergomard, J. P. Dalmont, J. Gilbert, P. Guillemain: Period doubling on cylindrical reed instruments. Proceeding of the Joint congress CFA/DAGA 04, 22nd-24th March 2004, Strasbourg, France, Société Française d'Acoustique - Deutsche Gesellschaft für Akustik, 113–114.

[6] P. Taillard, J. Kergomard, F. Laloë: Iterated maps for clarinet-like systems. Nonlinear Dyn. **62** (2010) 253–271.

[7] J. Kergomard, S. Ollivier, J. Gilbert: Calculation of the spectrum of self-sustained oscillators using a variable troncation method. Acta Acust. united Ac. **86** (2000) 665–703.

[8] J. P. Dalmont, J. Gilbert, J. Kergomard, S. Ollivier: An analytical prediction of the oscillation and extinction thresholds of a clarinet. J. Acoust. Soc. Am. **118** (2005) 3294–3305.

[9] D. H. Keefe: Physical modeling of wind instruments. Computer Music Journal **16** (1992) pp. 57–73.

[10] S. Farner, C. Vergez, J. Kergomard, A. Lizée: Contribution to harmonic balance calculations of self-sustained periodic oscillations with focus on single-reed instruments. J. Acoust. Soc. Am. **119** (2006) 1794.

[11] B. Bergeot, A. Almeida, B. Gazengel, C. Vergez, D. Ferrand: Response of an artificially blown clarinet to different blowing pressure profiles. J. Acoust. Soc. Am. **135** (2014) 479–490.

[12] F. Silva: Émergence des auto-oscillations dans un instrument de musique à anche simple. Dissertation. Université Aix-Marseille I, 2009.

[13] B. Bergeot, C. Vergez, A. Almeida, B. Gazengel: Prediction of the dynamic oscillation threshold in a clarinet model with a linearly increasing blowing pressure. Nonlinear Dyn. **73** (2013) 521–534.

[14] C. Baesens: Slow sweep through a period-doubling cascade: Delayed bifurcations and renormalisation. Physica D **53** (1991) 319–375.

[15] A. Fruchard, R. Schäfke: Bifurcation delay and difference equations. Nonlinearity **16** (2003) 2199–2220.

[16] B. Bergeot, C. Vergez, A. Almeida, B. Gazengel: Prediction of the dynamic oscillation threshold in a clarinet model with a linearly increasing blowing pressure: Influence of noise. Nonlinear Dyn. **74** (2013) 591–605.

[17] S. Ollivier, J. P. Dalmont, J. Kergomard: Idealized models of reed woodwinds. part 1 : Analogy with bowed string. Acta Acust. united Ac. **90** (2004) 1192–1203.

[18] A. Chaigne, J. Kergomard: Instruments à anche. – In: Acoustique des instruments de musique. Belin, 2008, Ch. 9, 400–468.

[19] B. Bergeot: Naissance des oscillations dans les instruments de type clarinette à paramètre de contrôle variable. Dissertation. Université du Maine, 2013.

[20] A. Almeida, B. Bergeot, C. Vergez: Attack transients in clarinet models with different complexity – a comparative view. Proceedings of the International Symposium in Music Acoustics, 2014, pp. 51–57.

[21] B. Bergeot, A. Almeida, C. Vergez: Effect of the shape of mouth pressure variation on dynamic oscillation threshold of a clarinet model. Proceedings of the International Symposium in Music Acoustics, 2014, pp. 535–540.

[22] I. S. Gradshteyn, I. M. Ryzhik: Table of integrals, series, and products (7th ed.). Academic Press, New York, 1965.